Wind and Structures, *Vol. 26, No. 2 (2018) 57-68*
DOI: https://doi.org/10.12989/was.2018.26.2.057

Experimental study on wake-induced vibrations of two circular cylinders with two degrees of freedom

Xiaoqing Du*[1], Benjian Jiang[1], Chin Dai[2], Guoyan Wang[3] and Suren Chen[4]

[1]*Department of Civil Engineering, Shanghai University, Shanghai, China*
[2]*Shanghai Institute of Applied Mathematics and Mechanics, Shanghai University, Shanghai, China*
[3]*School of Aerospace Engineering and Applied Mechanics, Tongji University, Shanghai, China*
[4]*Department of Civil and Environmental Engineering, Colorado State University, Colorado, United States*

(Received September 18, 2017, Revised December 7, 2017, Accepted December 9, 2017)

Abstract. Wind tunnel tests are conducted to investigate wake-induced vibrations of two circular cylinders with a center-to-center spacing of 4 diameters and attack angle varying from 0° to 20° for Reynolds numbers between 18,000 and 168,800. Effects of structural damping, Reynolds number, attack angle and reduced velocity on dynamic responses are examined. Results show that wake-induced vortex vibrations of the downstream cylinder occur in a wider range of the reduced velocity and have higher amplitudes in comparison to the vortex-induced vibration of a single circular cylinder. Two types of wake-induced instability phenomena with distinct dynamic characteristics are observed, which may be due to different generation mechanisms. For small attack angles like 5° and 10°, the instability of the downstream cylinder characterizes a one-degree-of-freedom (1-DOF) oscillation moving in the across-wind direction. For a large attack angle like 20°, the instability characterizes a two-degree-of-freedom (2-DOF) oscillation with elliptical trajectories. For an attack angle of 15°, the instability can transform from the 1-DOF pattern to the 2-DOF one with the increase of the Reynolds number. Furthermore, the two instabilities show different sensitivity to the structural damping. The 1-DOF instability can be either completely suppressed or reduced to an unsteady oscillation, while the 2-DOF one is relatively less sensitive to the damping level. Reynolds number has important effects on the wake-induced instabilities.

Keywords: two circular cylinders; wind tunnel test; wake-induced vibration; Reynolds number effect

1. Introduction

Cables of long-span cable-supported bridges are prone to various wind-induced vibrations due to their inherent characteristics of high flexibility, extremely low damping and relatively small mass, such as vortex-induced vibration, rain-wind-induced vibration, dry inclined cable vibration and the galloping of iced cable etc. When two or more cables are arranged close to each other, the downstream cable is susceptible to wake-induced vibrations (WIVs) under the wake interference of the upstream cable. Large-amplitude WIVs of parallel cables have been observed on both cable-stayed bridges and suspension bridges (Yoshimura 1992, Caetano 2007, Takeguchi and Fukunaga 2012). It is known that large-amplitude cable vibrations may cause damage to the anchorage and cable fatigue, deserving particular attention and more insightful studies. The occurrence possibility of WIVs increases as the span of the cable-supported bridge getting longer, and the cable getting more flexible.

WIVs of two circular cylinders have been investigated intensively due to its frequent occurrence under different circumstances, such as power lines, chimneys and bridge cables (Wardlaw *et al*. 1975, Ruscheweyh 1983, Zdravkovich 1988, Matsumoto *et al*. 1990, Ting *et al*. 1998, Tokoro *et al*. 2000, Fujino *et al*. 2011, Takeguchi and Fukunaga 2012, Li *et al*. 2013, Kim and Kim 2014, Yagi *et al*. 2015). As pointed out by Fujino and Siringoringo (2013), there exist three categories of WIV with different mechanisms for parallel cables, i.e., wake-induced vortex vibration (WIVV), wake galloping (WG) and wake-induced flutter (WIF). WIVV happens when the vortex shedding frequency of the upstream cable coincides with the oscillation frequency of the downstream one. WG and WIF are two types of aeroelastic instability phenomena with large amplitudes. WG is a one-degree-of-freedom (1-DOF) oscillation and the downstream cable vibrated mainly in the across-wind direction (see Fig. 1(a)). While WIF is a two-degree-of-freedom (2-DOF) oscillation and the downstream cable vibrates both in along- and across-wind directions with the dominant axis slightly inclined from the wind axis (see Fig. 1(b)). The occurrence of WG or WIF depends on the relative positions of two cylinders. The relative position of two cylinders is typically defined by the center-to-center spacing P between the cylinders, and the attack angle α denotes the orientation of the cylinders relative to the oncoming wind, see Fig. 1. Alternatively, the spacing P and the attack angle α can be replaced by the longitudinal and transverse spacing, L and T, respectively.

As for wake galloping, it is commonly regarded that it happens when two circular cylinders are arranged relatively close to each other at the spacing ratio of P/D=1.5-6 (D is the diameter of the cylinder). Numerous studies were

*Corresponding author, Associate Professor
E-mail: dxq@shu.edu.cn

ISSN: 1226-6116 (Print), 1598-6225 (Online)

conducted to investigate the instability and different generation mechanisms have been proposed. Paidoussis *et al*. (2011) suggested the mechanism of wake galloping is related to the galloping condition, in which instability occurs when the downstream cylinder has negative aerodynamic damping as described in Den Hartog criterion. Ruscheweyh and his coauthors (Ruscheweyh 1983, Ruscheweyh and Dielen 1992, Dielen and Ruscheweyh 1995) investigated experimentally and analytically the instability of two circular cylinders with small spacing ratios of P/D=1.2-3.0. They used the terminology "interference galloping" instead of "wake galloping" and pointed out that the instability is associated with hysteretic flow switching in the gap between the two cylinders. Furthermore, Matsumoto *et al*. (1990) identified two different instability types on the downstream cylinders: a 2-DOF elliptical oscillation for staggered arrangements of L/D=1.5-3.0, T/D=0.5-2.0 and a 1-DOF transverse oscillation for tandem arrangements of L/D=1.5-4.0, T/D=0.

They found that the generation of an accelerated gap flow between the two cylinders plays a vital role in the first type of instability. For the second one, they suggested that the unsteady effect of the gap flow and outer flow is the dominant cause, which is consistent to the explanation by Ruscheweyh (1983) and has also been confirmed recently by particle image velocimetry (PIV) measurements in wind tunnel tests (Kim and Kim 2014). After investigating aerodynamic instabilities of two, three and four parallel cables with P/D=2-4, Kubo (1995) suggested that the wake galloping has different mechanisms with P/D being smaller and larger than a critical value around 3.6. Instead of using a rigid sectional model in wind tunnel tests, Tokoro *et al*. (2000) adopted a full-scale aeroelastic twin cable models to examine dynamic response characteristics. They found the downstream cylinder was subjected to a large-amplitude instability of elliptical trajectory for the case of P/D=4.3 and α=15°, which was different from the instability phenomenon observed by Matsumoto *et al*. (1990) on two staggered cylinders.

As for wake-induced flutter, it is commonly regarded that it happens when two circular cylinders are arranged with much larger spacing of P/D=8-20 than that of wake galloping. As wake-induced flutter occurs when the two cylinders are located so far apart, there is virtually no aerodynamic interference between the cylinders (Matsumoto *et al*. 1990). Besides, the flow pattern around the cylinders essentially keeps unchanged throughout the oscillation. Hence, the generation mechanism of wake-induced flutter is much clearer in comparison to wake galloping. According to Paidoussis *et al*. (2011), when wake-induced flutter occurs, the downstream cylinder moves leeward to a flow region with a higher velocity than it opposes when it moves back upward. Therefore, the downstream cylinder experiences a higher drag force when it moves leeward than moving upward, and extracts energy from the flow and results in the instability eventually. Wake-induced flutter was first observed on bundled conductors, often referred to as sub-span oscillation (Wardlaw *et al*. 1975), and was later observed on parallel suspension cables of a suspension bridge as the cables becoming longer and more flexible (Takeguchi and Fukunaga 2012). More recently, Li *et al*. (2013) found that the instability could also occur on inclined stay cables. Wake-induced flutter is associated with the coupled flutter condition and can occur despite the positive aerodynamic damping condition (Paidoussis *et al*. 2011). Therefore, increasing structural damping is not effective in terms of suppressing the effects of wake-induced flutter (Price and Piperni 1988, Takeguchi and Fukunaga 2012, Hardy and Van Dyke 1995).

Despite the fact that wake galloping and wake-induced flutter of two cylinders have been studied extensively, there are still some issues needed to be addressed due to the complexities of the phenomena. Firstly, more studies are needed to explore the generation mechanisms of wake-induced instability especially when two circular cylinders are arranged closely, e.g., P/D<6. Traditionally, wake galloping is regarded as a 1-DOF vibration occurring in the spacing range of P/D=1.5-6, while wake-induced flutter happens with two degrees of freedom in P/D=8-20. However, 2-DOF instabilities were also identified in the spacing range of P/D<6 in previous literature. Secondly, Reynolds number effects on the wake-induced instabilities need more investigation. It is known that aerodynamics of and flow field around two static circular cylinders are particularly sensitive to the Reynolds number (Sumner 2010). However, most of the previous studies were conducted at relatively low subcritical Reynolds numbers, and there are limited studies conducted at high Reynolds numbers. Thirdly, wake-induced vortex vibration of two circular cylinders in the staggered arrangement with small spacing needs further research. Previous studies on wake-induced vortex vibration mostly focused on either two tandem cylinders (Wong 1980, Kim *et al*. 2009) or two staggered cylinders with large spacing (Brika and Laneville 1997).

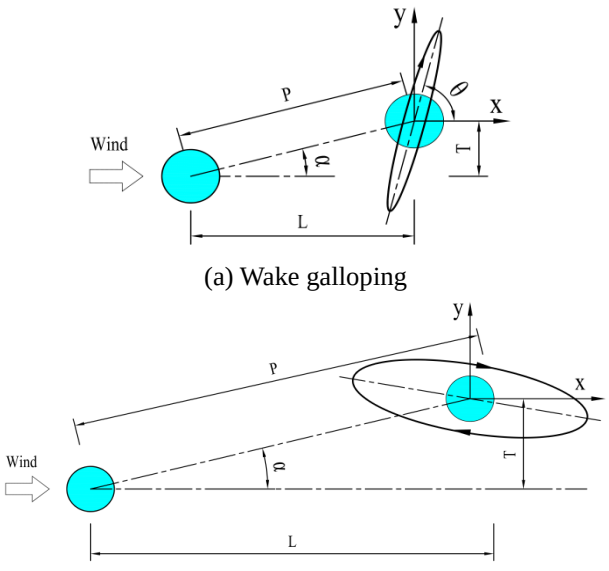

(a) Wake galloping

(b) Wake-induced flutter

Fig. 1 Typical trajectory of wake-induced instabilities

Table 1 Parameters of the wind tunnel test

Parameters	Values
Diameter of the cylinders, D (mm)	180
Weight of the downstream cylinder, m (kg/m)	12.6
Degrees of freedom	2 (along-wind and across-wind)
Natural frequency, f (Hz)	1.73
Attack angle, α	0°, 5°, 10°, 15°, 20°
Logarithmic damping decrement, δ	0.007, 0.026, 0.036, 0.058
Scruton number, Sc*	5, 17, 23, 38
Reynolds number, Re	18000 - 168800

*: Scruton number is defined as $Sc=2m\delta/\rho D^2$, where ρ is the air density

The present study aims to investigate experimentally the dynamic characteristics of wake-induced vortex vibration and wake-induced instabilities on two closely arranged circular cylinders at high subcritical Reynolds numbers of 18,000-168,800. Effects of Reynolds number, structural damping, attack angle and reduced velocity on the dynamic responses are examined. Two sectional circular cylinders with a spacing ratio of P/D=4 are adopted, and the attack angle varies from 0° to 20°. The upstream circular cylinder is stationary, while the downstream cylinder is supported by springs and could move in two degrees of freedom, i.e., both in along-wind and across-wind directions. Firstly, the responses of wake-induced vortex vibration are compared to those of vortex-induced vibration of a single circular cylinder. Secondly, the responses of wake-induced instabilities for different attack angles are obtained, and two different types of instability phenomena are identified. Dynamic response characteristics of the two instabilities, such as maximum amplitude, time history of response and oscillation trajectory, are studied. Reynolds number effects on the instabilities are discussed as well. Thirdly, effects of structural damping on wake-induced vortex vibrations and wake-induced instabilities are investigated.

2. Wind tunnel tests

To acquire relative high Reynolds numbers, two rigid sectional circular cylinders are used in the tests instead of aeroelastic models, which typically have small diameters.

The two cylinders are made from acrylic tubes and have the same diameter of D=180 mm. The Reynolds numbers based on the diameter of one single cylinder and the incoming wind velocity range from Re=18,000 to 168,800, which is located in the subcritical Reynolds number regime. Fig. 2 shows the schematic diagram of the experimental model. As shown in the figure, the two cylinders are mounted horizontally on set-up in the wind tunnel and are subjected to crosswind. The upstream cylinder is fixed on the set-up, which can be adjusted to acquire five attack angles of 0°, 5°, 10°, 15° and 20°. The downstream cylinder is supported by four springs at each end and can vibrate in both along-wind (x-direction) and across-wind (y-direction) directions with an almost identical frequency of f=1.73 Hz.

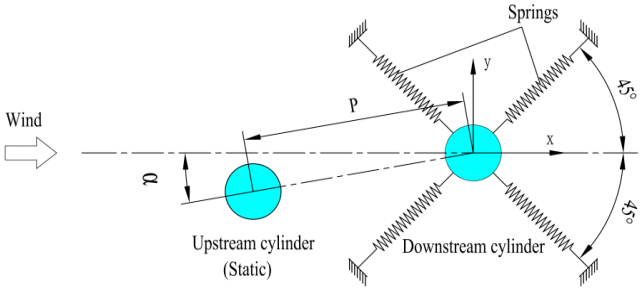

Fig. 2 Schematic diagram of the cable models

The center-to-center spacing of the two cylinders is four times of the diameter, i.e., P/D=4. In order to simulate two-dimensional flow conditions, each end of the cylinders is equipped with a circular end plate of a diameter of 3D. Besides, the upstream cylinder has a length of 7D while the downstream cylinder with a length of 6D. The experimental parameters of the wind tunnel test are listed in Table 1. To provide additional damping to the model system, thin steel wire rings are attached to the springs of the model. As the cable model vibrates, the wire rings deform correspondingly with the oscillation of springs and absorb the kinetic energy of the model. Thus, the damping level of the model system is lifted (Gu and Du 2005).

The tests were conducted in the wind tunnel laboratory at Shanghai University, which has a working section of 1.8 m width, 1.2 m height, and 18 m length. The effective wind speeds of the wind tunnel range from 0.2 to 30 m/s and the turbulence intensity is less than 1%. Considering the projected areas of the cylinder model, end plates, and the set-up, the area blockage ratio of the tests is about 11%. At the end of the downstream cylinder, accelerometers are deployed to measure the along-wind and across-wind movements of the cylinder, and the sampling frequency of the accelerometers is 100 Hz.

3. Results and discussion

3.1 Wake-induced vortex vibration

In order to discuss the differences between the WIVV and the vortex-induced vibration (VIV), the upstream circular cylinder was first removed to measure the VIV of a single circular cylinder. The relationship between the maximum amplitude of the VIV and the reduced velocity (*V/fD*) is shown in Fig. 3. Two dimensionless parameters, *X*/*D* and *Y*/*D*, are introduced to denote the maximum observed amplitudes of along-wind and across-wind movements respectively. As expected, the single cylinder suffers VIV at the reduced velocity (*V/fD*) between 5-7 where the frequency of vortex shedding is close to the structural frequency of the cylinder, and the lock-in phenomenon happens. The VIV reaches the peak amplitude of 0.18 at *V/fD* around 6, and the cylinder vibrates mainly in the across-wind direction.

As for two circular cylinders, Fig. 4 illustrates the maximum amplitudes of the WIVV as functions of the reduced velocity for the attack angle α of 0^o, 5^o, and 20^o. It can be seen from Fig. 4 that, similar to the VIV, WIVV of the downstream cylinder mainly happens in the across-wind direction even when the two cylinders are arranged in a staggered configuration. Meanwhile, the vibration responses of the WIVV also show some different characteristics in comparison with the VIV. For $\alpha=0^o$, 5^o, and 20^o, the amplitudes of the WIVV are much higher than those of the VIV. In the case of $\alpha=0^o$, the peak amplitude is up to 0.35, which is almost two times the peak value of the VIV. While for $\alpha=10^o$ and 15^o (the results have not presented here), the peak amplitudes of WIVV have the same level as those of the VIV. Furthermore, as for the range of reduced velocity where WIVV happens, the range is similar to that of the VIV for the case of $\alpha=0^o$, while the WIVV for $\alpha=5^o$ and 20^o takes place in a broader range of the reduced velocity than the VIV.

According to Alam and Meyer (2013), for two static circular cylinders being arranged at *P/D*=4 and $\alpha=0^o$ and 5^o, the interaction mechanism between the two cylinders belongs to "vortex and cylinder interaction regime". This kind of interaction intensifies fluctuating lift significantly on the downstream cylinder, which may result in a relatively high amplitude of WIVV. For the case of $\alpha=20^o$, the downstream cylinder immerses in a more asymmetrical flow field, which induces a significant lift force on the downstream cylinder.

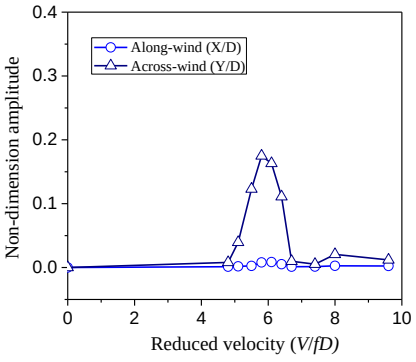

Fig. 3 Maximum amplitude of vortex-induced vibration (VIV) of a single circular cylinder (*Sc*=5)

Hence, it may be due to the combined effects of the asymmetrical flow field and the vortices produced by the upstream cylinder that the WIVV occurs in a broader range of the reduced velocity and results in higher amplitudes as compared to the VIV.

3.2 Wake-induced instabilities

With the reduced velocity increasing further beyond the WIVV lock-in region, the resonant effect is getting weaker. However, the downstream cylinder may experience wake-induced instability with oscillation amplitudes much higher than those of the WIVV.

3.2.1 Effects of attack angle on the instabilities

Fig. 5 presents the maximum amplitude of wake-induced vibration against the reduced velocity and Reynolds number for the attack angle α of 0^o, 5^o, 10^o, 15^o and 20^o. As shown in the figure, when the reduced velocity is higher than 7 or 8, except for the case $\alpha=0^o$, large amplitude wake-induced instabilities happen for the rest of four other cases.

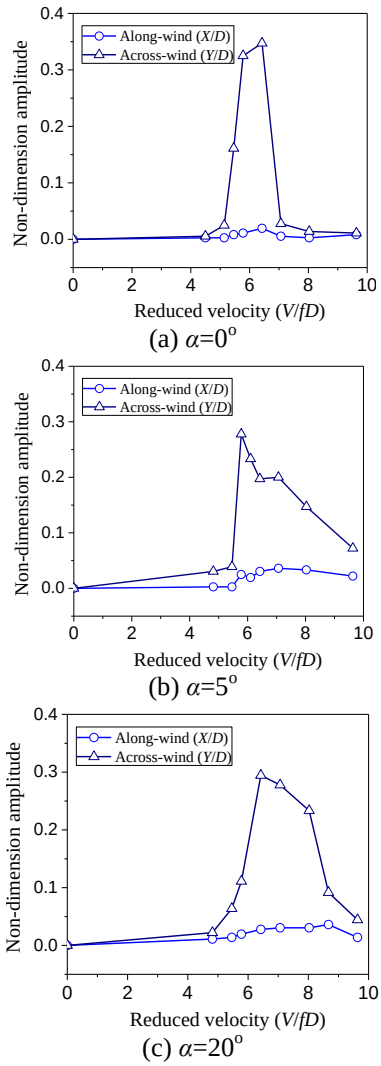

Fig. 4 Maximum amplitude of wake-induced vortex vibration with *Sc*=5

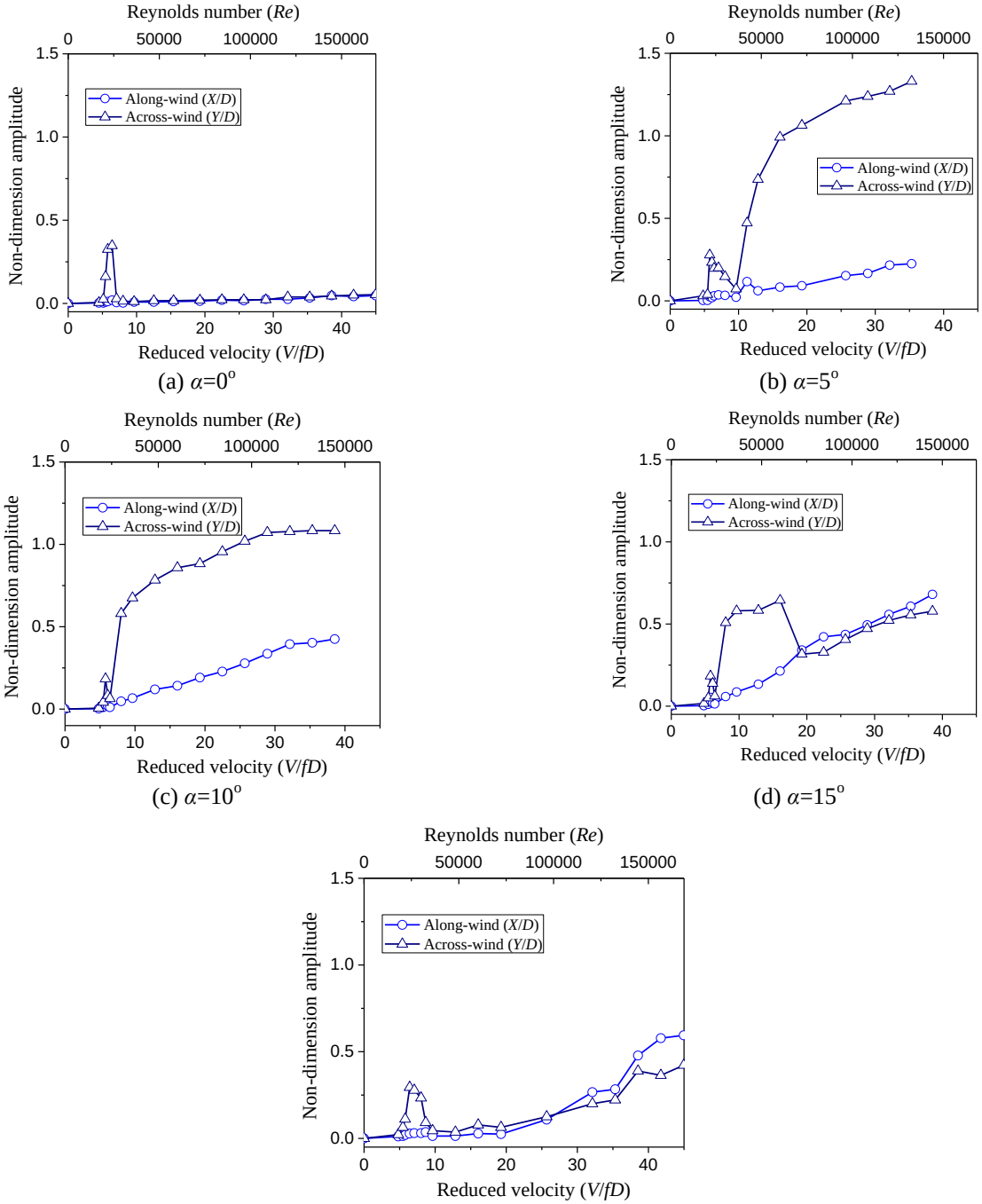

Fig. 5 Maximum amplitude of wake-induced vibration (WIV) with *Sc*=5

Fig. 5(a) presents the maximum amplitudes of the displacements for the two cylinders arranged in a tandem configuration (α=0°). The downstream cylinder vibrates noticeably only in the synchronization range when the reduced velocity is around 6, and there is no large-amplitude wake-induced instability observed in the tests. This result is in agreement with that by Tokoro *et al*. (2000) and Fujino *et al*. (2011), in which no instability phenomenon for two tandem cylinders with the spacing ratio similar to the present study was observed. However, some literature (e.g., Kim 2014, Yagi 2015) stated wake-induced instability phenomena for two tandem cylinders with *P/D* around 4 were observed. The reason for the discrepancy may be due to the differences of parameters adopted in the tests, such as mass, damping, and Reynolds number *et al*.

For α=5° (see Fig. 5(b)), the downstream cylinder shows a large-amplitude divergent-type oscillation at the reduced velocity beyond the synchronization.

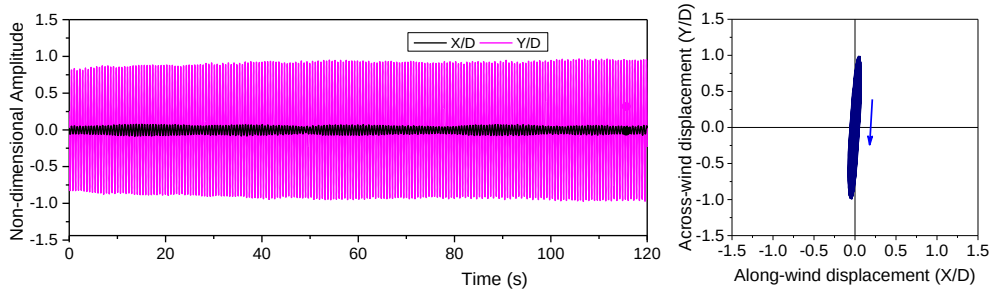

(a) α=5°, V/fD=16

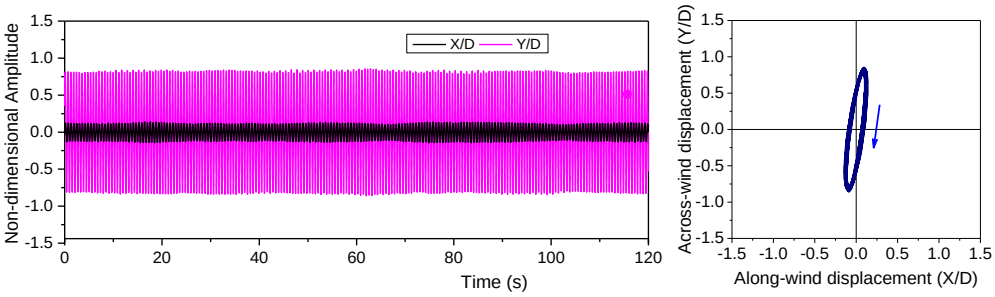

(b) α=10°, V/fD=16

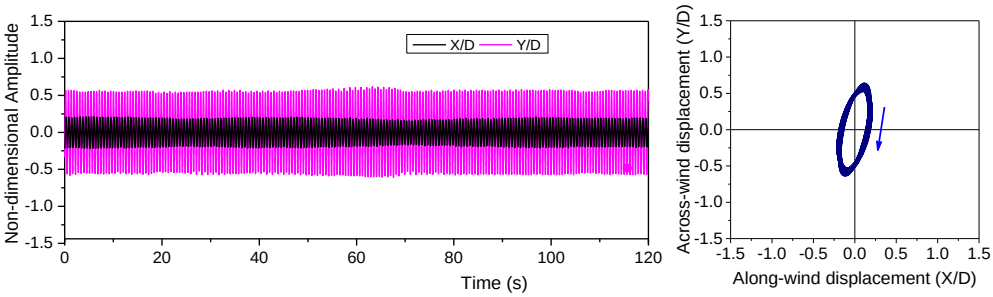

(c) α=15°, V/fD=16

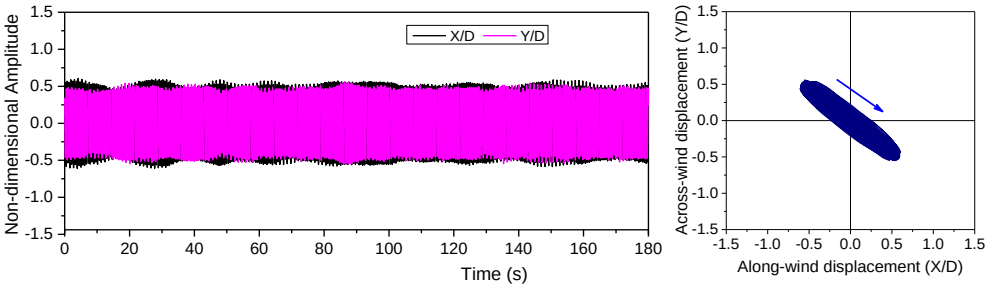

(d) α=15°, V/fD=35

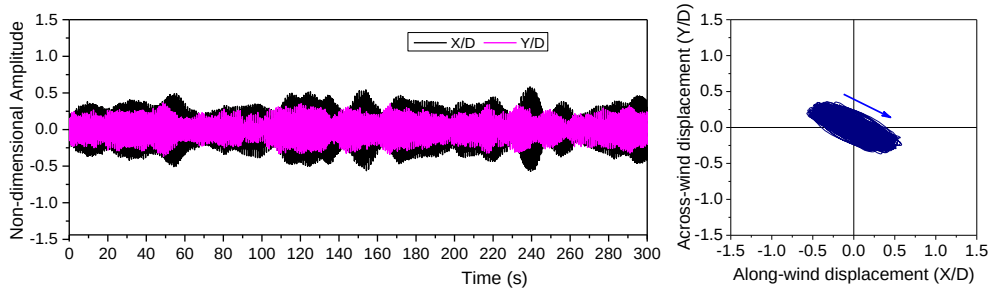

(e) α=20°, V/fD=42

Fig. 6 Time history of dynamic responses of instability (left) and its trajectory (right) with Sc=5

The across-wind amplitudes are much higher than the along-wind one, which is a typical dynamic characteristic of wake galloping. The cylinder begins to oscillate at a reduced velocity around 8 and the vibration amplitude increases quickly to a level higher than 1*D* when the reduced velocity keeps growing. At the reduced velocity of 35, the amplitude reaches the allowable limits that can be accommodated by the test facility. With the attack angle increasing to α=10^o, as shown in Fig. 5(c), the dynamic characteristics of the downstream cylinder show small changes as compared to those of the case of α=5^o. The onset reduced velocity of the vibration decreases slightly, and the cylinder begins to undergo large amplitude vibration at a reduced velocity as low as 8, which is followed closely by the synchronization range. As for the amplitude of the vibration, the across-wind amplitudes reduce slightly, and the along-wind ones increase a little. In general, the large dynamic responses for the cases of α=5^o and 10^o are similar and occur mainly in the transverse direction.

When the attack angle increases further to α=15^o, the vibration characteristics change significantly, as observed in Fig. 5(d). The instability occurs at the reduced velocity around 8, and the vibration characteristics are similar to those of α=10^o, with the transverse response much larger than longitudinal one. Nevertheless, after the instability occurs, the amplitudes of the vibration have not kept growing with the increase of the reduced velocity as expected. The amplitude of transverse vibration falls suddenly to the level of longitudinal vibration when the reduced velocity reaches 20. Moreover, the trajectories of the vibration also change dramatically, which will be discussed further in the next section.

For α=20^o (see Fig. 5(e)), the downstream cylinder oscillates differently in comparison with the cases of α=5^o and 10^o. The onset velocity of the wake-induced instability is higher than that in Figs. 5(b)-5(d). Furthermore, the cylinder vibrates both in across-wind and along-wind directions with similar levels of the transverse amplitude. Furthermore, it will be shown in the next section that the dominant axis direction of the vibration is different from those of α=5^o and 10^o.

These differences of the dynamic characteristics between the small attack angles (α=5^o and 10^o) and the large one (α=20^o) indicate that there may exist two types of wake-induced instability phenomena with different mechanisms.

3.2.2 Time history of the instabilities

To understand the difference between the two possible different instabilities, dynamic response characteristics of the downstream cylinder are further studied. Fig. 6 illustrates typical time histories of the displacement (left) of the downstream cylinder and corresponding oscillation trajectories (right) for attack angles α=5^o, 10^o, 15^o and 20^o at reduced velocities where wake-induced instabilities happen.

The trajectories are obtained when the vibration of the downstream cylinder has reached the limit cycles. Figs. 6(c)-(d) show responses at two reduced velocities of *V/fD*=16 and 35 for α=15^o.

For α=5^o, 10^o, 15^o at *V/fD*=16, it can be seen from the displacement time history in Fig. 6 (left) that the responses are quite steady with the maximum amplitude keeping nearly unchanged. As for the vibratory trajectory, at the wind attack angle of α=5^o, we can see from Fig. 6(a) (right) that the downstream cylinder oscillates mainly in the across-wind direction. However, with the increase of the attack angle, the along-wind amplitude of the cylinder increases gradually but remains smaller than the across-wind one. Meanwhile, the dominant axis of the vibration direction rotates gently in the clockwise direction.

As mentioned above that, for α=15^o, the maximum amplitude does not grow continually with the velocity after the wake-induced instability happens. On the contrary, the amplitude of transverse vibration falls suddenly when the reduced velocity increases from 16 to 20. Figs. 6(c) and 6(d) present the dynamic responses and the vibratory trajectories of the instability for α=15^o with *V/fD* of 16 and 35, respectively. We can see from the figures that the dominant axis of the vibration direction changes significantly with the increase of the reduced velocity. For the lower reduced velocity, the downstream cylinder oscillates vertically with the across-wind amplitude much larger than the along-wind one. However, for higher reduced velocities, the cylinder oscillates obliquely with the across-wind response smaller than the along-wind one.

For α=20^o, as shown in Fig. 6(e), the time history of dynamic response appears rather unsteady with the maximum amplitude fluctuating considerably in comparison with other cases. The downstream cylinder oscillates elliptically with the angle between the oncoming wind and the dominant vibratory axis distinctly different from those of small attack angles, α=5^o and 10^o.

3.2.3 Oscillation trajectory of the instabilities

To investigate the effects of the reduced velocity and Reynolds number on the oscillation pattern of two different instabilities, oscillation trajectories of the downstream cylinder for the cases of α=5^o and 15^o are illustrated in Fig. 7 at various reduced velocities and Reynolds numbers.

For α=5^o (see Fig. 7(a)), the maximum amplitude of the oscillation increases with the growth of wind speed, while the dominant axes of oscillation are slightly inclined toward the across-wind direction. However, with the reduced velocity and Reynolds number increasing to *V/fD*=29 and *Re*=1.1×10^5 respectively, the center of the trajectory moves to *x*/*D*=-0.12 and *y*/*D*=-0.02, which indicates the downstream cylinder is attracted by the upstream cylinder and exhibits a noticeable static displacement. The phenomenon may occur due to the Reynolds number effects on the flow field between the two cylinders. As for two static tandem circular cylinders (*T*=0), there exists a critical pitch ratio $(L/D)_c$ between 3.5 to 5 where the flow pattern around the cylinders switches from the reattachment regime to the co-shedding regime (Xu and Zhou 2004). Accordingly, the downstream cylinder experiences a discontinuous jump from a negative drag coefficient to a positive mean drag coefficient with the increase of pitch ratio. The critical pitch is particularly sensitive to the Reynolds number. Furthermore, according to Ljungkrona

and Sunden (1993), at Reynolds number around 10^5, the critical pitch ratio $(L/D)_c$ increases slightly from around 3.6 to 3.8 with the increase of Reynolds number. In the present study, considering the inclination of the dominant axis of oscillation, the longitudinal spacing ratio L/D between the two cylinders is less than 4 as the downstream cylinder moves across the wake centreline of the upstream cylinder. Therefore, with the increase of Reynolds number, the critical pitch increases and the shear layers from the upstream cylinder may reattach onto the downstream cylinder intermittently during the oscillation, which causes the downstream cylinder to undergo negative drag and the noticeable static displacement.

For α=15°, as shown in Fig. 7(b) and mentioned above, the trajectories of the oscillation change significantly with the increase of the reduced velocity and Reynolds number. For the low reduce velocity, V/fD=10, and Re=3.6×10^4, the downstream cylinder oscillates in nearly vertical direction, while for the high ones, V/fD>19 and Re>7.2×10^4, the cylinder vibrates both in vertical and transverse directions with the dominant response direction rotating to the upstream direction. For the case of V/fD=19 and Re=7.2×10^4, the oscillation of the downstream cylinder is at an intermediate state between these two patterns with a roughly circular trajectory.

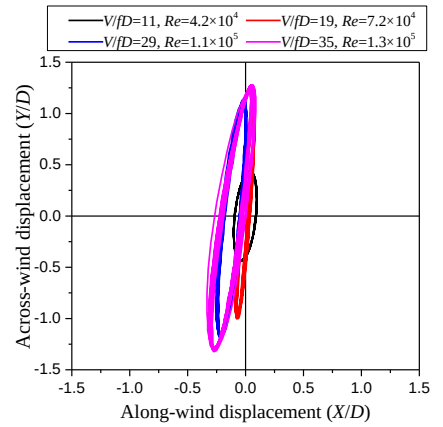

(a) α=5°

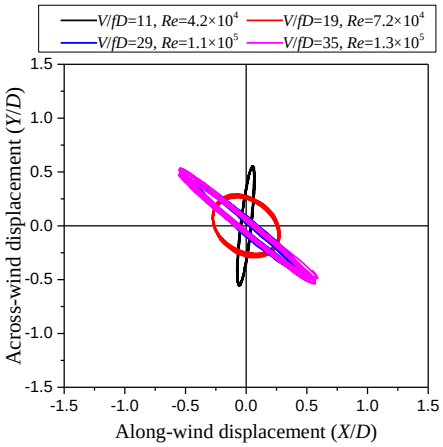

(b) α=15°

Fig. **7** Oscillation trajectory against reduced velocity and Reynolds number (Sc=5)

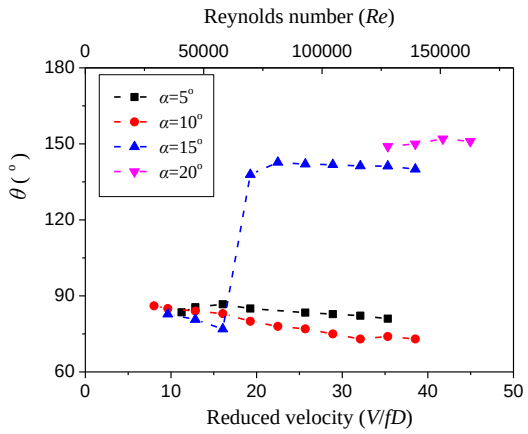

Fig. 8 The relationship of vibration direction and reduced velocity (Sc=5)

Furthermore, Fig. 8 illustrates the relationship of vibration direction and reduced velocity when the vibrations reach their limit cycle. The vibration direction is defined by the angle between wind axis and vibration dominant axis θ (see Fig. 1). It can be seen from Fig. 8 that the angle θ is divided into two branches: a lower one between 60° to 90° corresponding to small wind angles and an upper one between 120° to 150° corresponding relatively large wind angles. For the lower branch, the angle θ decreases gradually with the increase of the reduced velocity. While for the upper branch, the angle θ has small change with the increase of the reduced velocity. As for α=15°, it is the critical wind angle where the angle θ jumps from the lower branch to the upper one as the reduced velocity increases to a specific value.

The reason for the transition of the oscillation pattern for α=15° may be related to the switch of two different flow patterns around the cylinders. As for two static circular cylinders, flow pattern around the cylinders is governed by three most important variables: the spacing between the cylinders, the attack angle and Reynolds number (Sumner 2010). When the spacing between the two cylinders is fixed as 4D in the present study, the flow around the cylinders is sensitive to the attack angle and Reynolds number. In addition, during the oscillation of the downstream cylinder, the amplitude of the oscillation will also affect the flow pattern as well. Therefore, there exists the combined effect of Reynolds number and oscillation amplitude that makes the oscillation pattern to transform from one pattern to another for the case of α=15°.

3.2.4 Evolvement of the instabilities

Fig. 9 illustrates dynamic response time histories and oscillation trajectories within the various time range for the cases of α=5° at V/fD=19 and α=15° at V/fD=39 respectively. It is found that the two types of instability evolved in different ways as the downstream cylinder began to vibrate from its original equilibrium position. It takes much longer time for the oscillation to reach the limit cycle for the cases of α=5° than for α=15°. Also, the evolvement of the instability for the small attack angle is more complicated than that for larger attack angles.

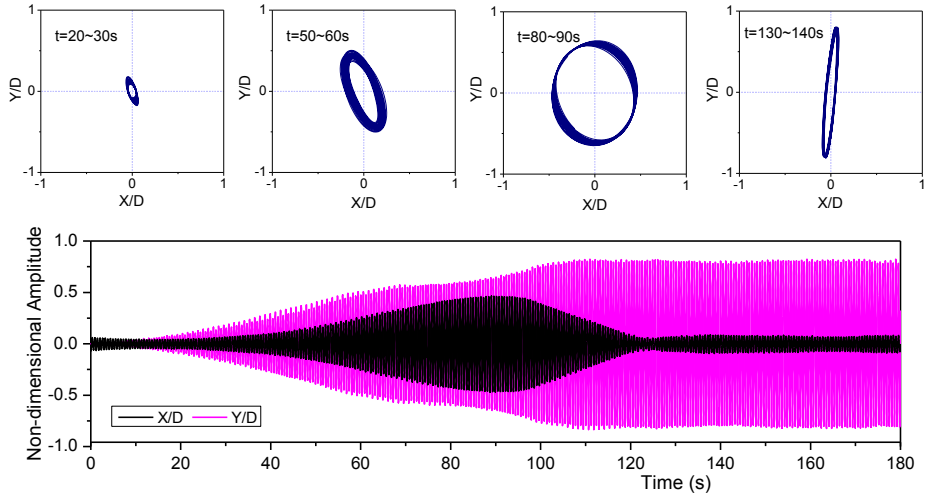

(a) α=5^o and V/fD=19

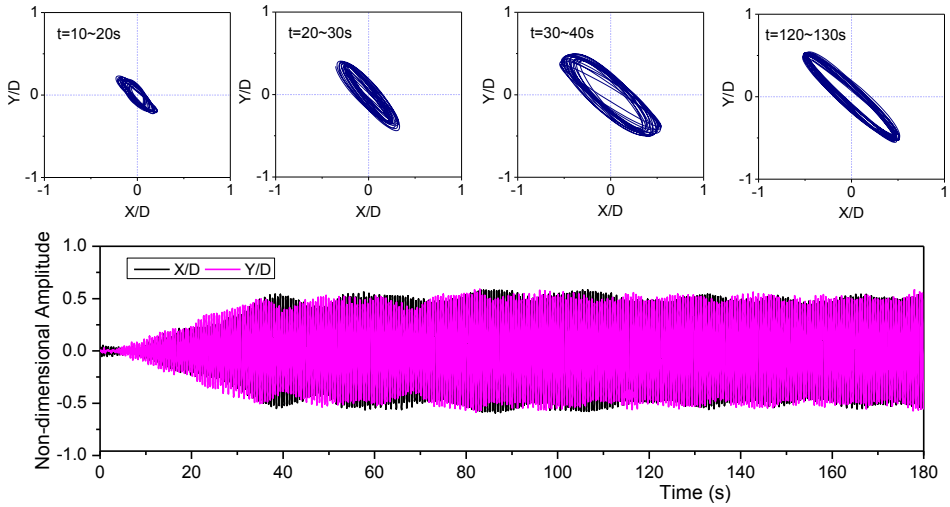

(b) α=15^o and V/fD=39

Fig. 9 Evolvement of instability with Sc=5

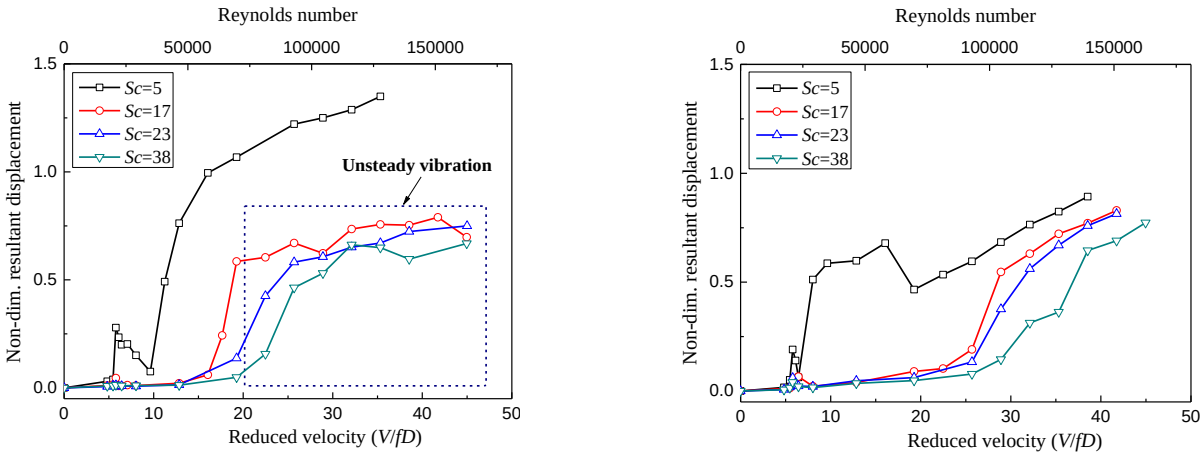

(a) α=5^o (b) α=15^o

Fig. 10 Effects of structural damping on wake-induced vibration

For α=5° (see Fig. 9(a)), the across-wind amplitude increases monotonically to a higher level. However, the along-wind amplitude increases gradually first at the early stage of oscillation within the time range of 20-90s and then decreases quickly to a low level after it reaches the peak at the time around the 90s. Furthermore, the pattern of oscillation trajectory also changes during the evolvement of the instability. For α=15° (see Fig. 9(b)), the evolvement of the instability appears straightforward with both along-wind and across-wind amplitudes monotonically increasing to a steady level, and the pattern of oscillation is similar at various time ranges. The phenomena suggest that the downstream cylinder may experience different flow patterns during the evolvement of the instability for the small attack angle. While for the large attack angle, the flow pattern around the downstream cylinder is unchanged.

3.3 Effects of structural damping

In order to investigate the mitigation effects of structural damping on WIV, four different levels of logarithmic damping decrement were adopted in the test, δ=0.007, 0.026, 0.036 and 0.058, which correspond to *Sc* of 5, 17, 23 and 38 approximately. Fig. 10 illustrates the impacts of damping on the resultant maximum amplitude of the vibration for α=5° and 15°. Here, the non-dimensional resultant amplitudes are obtained by $\sqrt{X^2+Y^2}/D$. Figs. 11 and 12 present the effects of damping on time history of dynamic response of the downstream cylinder at typically reduced velocities for α=5° and 15°.

As shown in Fig. 10, WIVV, which occurs at the reduced velocity around 6, can be efficiently suppressed by increasing the damping level for both wind angles. Even a damping level of δ=0.026 (*Sc*=17) can reduce the amplitude significantly. On the other hand, the effects of the damping on wake-induced instabilities are complicated.

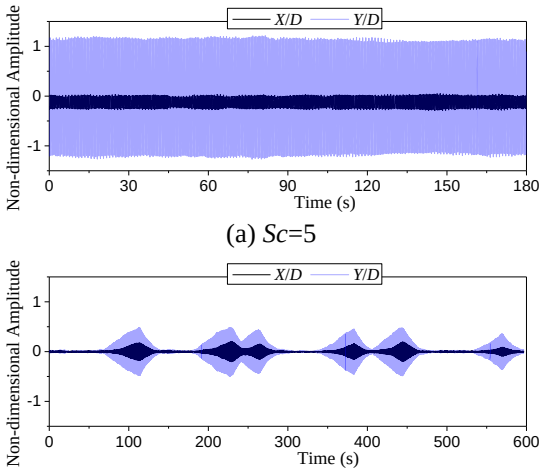

(a) *Sc*=5

(b) *Sc*=38

Fig. 11 Effects of damping on time history of response for α=5°, *V/fD*=29

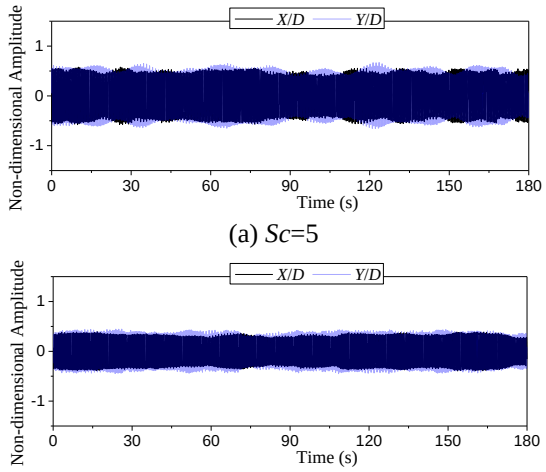

(a) *Sc*=5

(b) *Sc*=38

Fig. 12 Effects of damping on time history of response for α=15°, *V/fD*=39

For α=5° (see Fig. 10(a)), with the increase of damping level, the critical reduced velocity under which wake-induced instability occurs increases and the maximum amplitude of the vibration reduces. Fig. 11 illustrates the time histories of response at the reduced velocity of 29 for *Sc*=5 and 38. It can be seen from Fig. 11(a) that the vibration response of the downstream cylinder becomes rather steady once the instability happens for *Sc*=5. However, for *Sc*=38 (see Fig. 11(b)), the vibration response varies more randomly and intermittently with much lower amplitudes. It should be noted that, for the case of α=10° (the result is not presented here), the instability phenomenon is completely suppressed when Scruton number increases to 17, and unsteady responses cannot be observed.

For α=15° (see Fig. 10(b)), damping has different effects on the two kinds of instabilities happening at low velocities and high ones respectively. For the instability occurring between *V/fD*=8-19 and oscillating mainly in across-wind direction, it is effectively suppressed when the damping level is increased, and there is no unsteady vibration observed. For the instability occurring at *V/fD*>19, it cannot be suppressed entirely by the increase of damping. Although the maximum amplitudes reduce a little when the Scruton number is increased from 5 to 38, the time history of the vibration still keeps rather steady, as shown in Fig. 12.

Based on the results presented above, it may be concluded that there exist two types of wake-induced instability phenomena with fundamentally different dynamic response characteristics, such as maximum amplitude, time history of response and oscillation trajectory. For small attack angles like 5° and 10°, the instability of the downstream cylinder is governed by wake galloping mechanism, which characterizes a one-degree-of-freedom oscillation mainly in across-wind direction and can be either completely suppressed or reduced to an unsteady oscillation. It may be due to the alternate shift of flow pattern around the downstream cylinder that sustains the wake galloping instability. For a large attack angle such as

20^o, the instability phenomenon characterizes a two-degree-of-freedom oscillation with elliptical trajectory, which might be governed by wake-induced flutter mechanism and is relatively less sensitive to the damping level. For an attack angle of 15^o, wake-induced instability can transform from wake galloping into wake-induced flutter with the increase of Reynolds number and oscillation amplitude.

4. Conclusions

Wind tunnel tests are conducted to study wake-induced vibration of two circular cylinders with spacing ratio P/D=4 and attack angle α=0°-20° in the Reynolds numbers between 18,000 and 168,800. Efforts have been devoted to clarifying dynamic response characteristics of different types of wake-induced vibration. The effects of Reynolds number and the structural damping on the wake-induced vibrations are discussed as well. Several major findings are summarized in the following.

- The maximum amplitudes of wake-induced vortex vibration are generally higher in a synchronization range than those of the vortex-induced vibration of one single cylinder. As the attack angle increases, wake-induced vortex vibration was found to occur in a broader range of the reduced velocity as compared to the vortex-induced vibration.
- As the reduced velocity increases beyond the synchronization range, wake-induced instabilities of the downstream cylinder are observed when two cylinders are arranged in staggered configurations. It is found that there exist two types of wake-induced instability phenomena with different dynamic response characteristics, such as maximum amplitude, time history of response and oscillation trajectory. Results also show that Reynolds number has essential effects on the dynamic responses of wake-induced instability.
- For small attack angles like 5o and 10o, the wake-induced instability of the downstream cylinder characterizes a 1-DOF oscillation mainly in across-wind direction. For a large attack angle like 20o, the instability phenomenon characterizes a 2-DOF oscillation with elliptical trajectory. For an attack angle of 15o, the instability can transform from the former pattern to the later with the increase of Reynolds number and oscillation amplitude.
- Different types of wake-induced vibration show different sensitivity to the increase of structural damping. Wake-induced vortex vibration is easy to be suppressed by lifting the damping level, while the effects of the damping on wake-induced instability are complicated. The 1-DOF instability occurring at small attack angles can be either completely suppressed or mitigated to an unsteady oscillation with a significant decrease in amplitude, while the 2-DOF instability occurring at large attack angles is relatively less sensitive to the damping levels.

It should be mentioned that four parallel cables are commonly used in suspension bridges as the main span getting longer. Their characteristics of wake-induced vibration may be different from those of two cables and should be studied further. Others issues, such as the effects of the inclination of the stay cable, the free-stream turbulence, the surface roughness among others, are needed to be concerned as well.

Acknowledgments

We are thankful for the grants from National Natural Science Foundation of PRC (51578330), Innovation Program of Shanghai Municipal Education Commission (14YZ004) and Natural Science Foundation of Shanghai (14ZR1416000).

References

Alam, M.M. and Meyer, J.P. (2013), "Global aerodynamic instability of twin cylinders in cross-flow", *J. Fluid. Struct.*, **41**(8), 135-145.

Brika, D. and Laneville, A. (1997), "Vortex-induced oscillations of two flexible circular cylinders coupled mechanically", *J. Wind Eng. Ind. Aerod.*, **69**(97), 293-302.

Caetano, E. (2007), "Cable vibrations in cable stayed bridges", *Structural Engineering Documents 9*, IABSE-AIPC IVBH, Zurich Switzerland.

Dielen, B. and Ruscheweyh, H. (1995), "Mechanism of interference galloping of two identical circular cylinders in cross-flow", *J. Wind Eng. Ind. Aerod.*, **54-55**, 289-300.

Fujino, Y., Kimura, K. and Tanaka, H. (2012), "Cable vibrations and control methods. In: wind resistant design of bridges in Japan", Springer Japan, 197-229.

Fujino, Y. and Siringoringo, D. (2013), "Vibration mechanisms and controls of long-span bridges: a review", *Struct. Eng. Int.*, **23**(3), 248-268.

Gu, M. and Du, X. (2005), "Experimental investigation of rain-wind-induced vibration of cables in cable-stayed bridges and its mitigation", *J. Wind Eng. Ind. Aerod.*, **93**(1), 79-95.

Hardy, C. and Dyke, P.V. (1995), "Field observations on wind-induced conductor motions", *J. Fluid. Struct.*, **9**(1), 43-60.

Kim, S., Alam, M.M., Sakamoto, H. and Zhou, Y. (2009), "Flow-induced vibrations of two circular cylinders in a tandem arrangement. Part 1: Characteristics of vibration", *J. Wind Eng. Ind. Aerod.*, **97**(5-6), 304-311.

Kim, S. and Kim, H.K. (2014), "Wake galloping phenomena between two parallel/unparallel cylinders", *Wind Struct.*, **18**(5), 511-528.

Kubo, Y., Nakahara, T. and Kato, K. (1995), "Aerodynamic behavior of multiple elastic circular cylinders with vicinity arrangement", *J. Wind Eng. Ind. Aerod.*, **54-55**, 227-237.

Li, Y., Wu, M., Chen, X., Wang, T. and Liao, H. (2013), "Wind-tunnel study of wake galloping of parallel cables on cable-stayed bridges and its suppression", *Wind Struct*., **16**(3), 249-261.

Ljungkrona, L. and Sunden, B. (1993), "Flow visualization and surface pressure measurement on two tubes in an inline arrangement", *Exp. Therm. Fluid Sci.*, **6**(1), 15-27.

Matsumoto, M., Shiraishi, N. and Shirato, H. (1990), "Aerodynamic instabilities of twin circular cylinders", *J. Wind Eng. Ind. Aerod.*, **33**(1-2), 91-100.

Païdoussis, M.P., Price, S.J. and De Langre, E. (2011), *Fluid-structure interactions: Cross-flow-induced instabilities*, Cambridge University Press, UK.

Price, S.J. and Piperni, P. (1988), "An investigation of the effect of mechanical damping to alleviate wake-induced flutter of overhead power conductors", *J. Fluid. Struct.*, **2**(1), 53-71.

Ruscheweyh, H.P. (1983), "Aeroelastic interference effects between slender structures", *J. Wind Eng. Ind. Aerod.*, **14**(1-3), 129-140.

Ruscheweyh, H. and Dielen, B. (1992), "Interference galloping-investigations concerning the phase lag of the flow switching", *J. Wind Eng. Ind. Aerod.*, **43**(1-3), 2047-2056.

Sumner, D. (2010), "Two circular cylinders in cross-flow: a review", *J. Fluid. Struct.*, **26**(6), 849-899.

Takeguchi, M. and Fukunaga, S. (2012), "Aerodynamic stabilization for wake-induced vibration in parallel hanger ropes of the Akashi Kaikyo Bridge", *Wind Eng. JAWE*, **37**(4), 300-306. (in Japanese)

Ting, D.K., Wang, D.J., Price, S.J. and Paidoussis, M.P. (1988), "An experimental study on the fluidelastic forces for two staggered circular cylinders in cross-flow", *J. Fluid. Struct.*, **12**(3), 259-294.

Tokoro, S., Komatsu, H., Nakasu, M., Mizuguchi, K. and Kasuga, A. (2000), "A study on wake-galloping employing full aeroelastic twin cable model", *J. Wind Eng. Ind. Aerod.*, **88**(2-3), 247-261.

Wardlaw, R.L., Cooper, K.R., Ko, R.G. and Watts, J.A. (1975), "Wind tunnel and analytical investigations into the aeroelastic behavior of bundled conductors", *IEEE T. Power Apparatus Syst.*, **94**(2), 642-654.

Wong, H.Y. (1980), "Vortex-induced wake buffeting and its suppression", *J. Wind Eng. Ind. Aerod.*, **6**(1-2), 49-57.

Xu, G. and Zhou, Y. (2004), "Strouhal numbers in the wake of two inline cylinders", *Exp. Fluids*, **37**(2), 248-256.

Yagi, T, Arima, M., Araki, M., *et al*. (2015), "Investigation on wake-induced instabilities of parallel circular cylinders based on unsteady aerodynamic forces", *Proceedings of the 4th International Conference on Wind Engineering*, Porto Alegre, Brazil.

Yoshimura, T. (1992), "Aerodynamic stability of four medium span bridges in Kyushu district", *J. Wind Eng. Ind. Aerod.*, **42**(1-3), 1203-1214.

Zdravkovich, M.M. (1988), "Review of interference-induced oscillations in flow past two parallel circular cylinders in various arrangements", *J. Wind Eng. Ind. Aerod.*, **28**(1-3), 183-199.

CC